arXiv:1607.08800v1 [cond-mat.mes-hall] 29 Jul 2016

Recovery of a SINIS turnstile accuracy in a strongly non-equilibrium regime

I. M. Khaymovich[1,2,3] and D. M. Basko[1]

[1] *Laboratoire de Physique et Modélisation des Milieux Condensés, Université de Grenoble Alpes and CNRS, 25 rue des Martyrs, 38042 Grenoble, France*
[2] *Nanosciences Foundation, 23 rue des Martyrs, 38000 Grenoble, France*
[3] *Institute for Physics of Microstructures, Russian Academy of Sciences, 603950 Nizhny Novgorod, GSP-105, Russia*

(Dated: August 1, 2016)

We perform a theoretical study of non-equilibrium effects in charge transport through a hybrid single-electron transistor based on a small normal metal (N) island with the gate-controlled number of electrons, tunnel-coupled to voltage-biased superconducting (S) electrodes (SINIS). Focusing on the turnstile mode of the transistor operation with the gate voltage driven periodically, and electrons on the island being out of equilibrium, we find that the current quantization accuracy is a non-monotonic function of the relaxation rate $\Gamma_{\mathcal{F}}$ of the distribution function $\mathcal{F}(\epsilon)$ on the island due to tunneling, as compared to the drive frequency f, electron-electron $1/\tau_{ee}$ and electron-phonon $1/\tau_{eph}$ relaxation rates. Surprisingly, in the strongly non-equilibrium regime, $f \gg \Gamma_{\mathcal{F}} \gg \tau_{ee}^{-1}, \tau_{eph}^{-1}$, the turnstile current plateau is recovered, similarly to the ideal equilibrium regime, $\tau_{eph}^{-1} \gg \Gamma_{\mathcal{F}}$. The plateau is destroyed in the quasiequilibrium regime when the electron-electron relaxation is faster than tunneling.

I. INTRODUCTION

Nowadays, hybrid superconducting systems play an important role in several domains of physics and technology such as electronic refrigeration[1], metrology[2] etc. One aspect, widely addressed in the literature, is the overheating of the superconducting (S) parts of hybrid junctions as they can be easily driven out of equilibrium under typical operating conditions (see, e.g., Ref. 3). When overheated, superconducting parts contain many hot quasiparticles (QPs) which compromise the performance of mesoscopic devices.[4] To overcome the problem of hot QPs, quite a number of efforts have been made to reduce these overheating effects in S by putting different types of quasiparticle traps[12–17] and by cooling S-parts directly.[18–21] Despite some pessimistic theoretical predictions of the residual QP densities,[22] these efforts have been rather successful as the quasiparticle densities were indeed remarkably reduced there.[3,16,23–25]

Besides the problem of hot QPs in the superconductors, which is partly solved, there is a question of electron overheating in the normal metal (N) parts of mesoscopic devices. The relaxation rates in N parts are significantly faster than in S; nevertheless, there are both theoretical and experimental studies of the non-equilibrium distributions in N wires,[26] in single-electron transistors,[27] and in N parts of NIS coolers[28,29] where 'I' stands for insulator. Under experimentally achievable conditions, the electronic energy distribution $\mathcal{F}(\epsilon)$ in the normal metal can have non-Fermi-Dirac form, which leads to measurable consequences.

In this paper, we address the problem of non-equilibrium electronic distributions in a similar type of device, namely, in a hybrid superconducting single-electron transistor (SET) consisting of a small metallic normal island, sandwiched between two superconducting electrodes. Such configuration, usually called SINIS, is shown schematically in Fig. 1. Under equilibrium conditions, a large Coulomb energy (compared to the bath temperature T) prevents an extra electron from tunneling into the island, which enables one to control the electron number n of the island by applying a voltage to a nearby gate electrode.

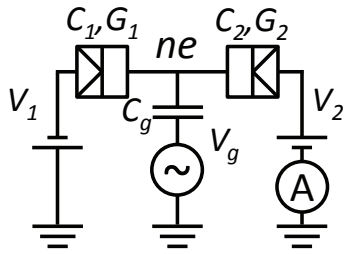

FIG. 1. Schematics of a hybrid SINIS SET used in turnstile experiments.

One way to drive a SINIS SET out of equilibrium is to apply a periodic driving gate voltage in the so-called turnstile regime,[30] which has potential applications in quantum metrology.[2,31] Then, one measures the charge current $\langle I \rangle$ through the device, averaged over the drive period. A hybrid superconducting turnstile was realized for the first time in Ref. 30. It is a voltage-biased hybrid SINIS SET working as schematically shown in Fig. 2. By applying a periodic voltage to the gate electrode with a driving frequency f, one can change the chemical potential μ of the normal island (see the two positions of $\mu(t)$ in panels (a) and (b) of the figure). Due to the Coulomb interaction, in a certain range of the gate voltage amplitudes only two charge states of the island are available. Therefore, when μ is aligned with the lower quasiparticle branch below the gap of the left electrode, one electron is loaded to the island from the left electrode, see panel (a), while when μ is above the gap of the right electrode, an electron tunnels out from the island to the right elec-

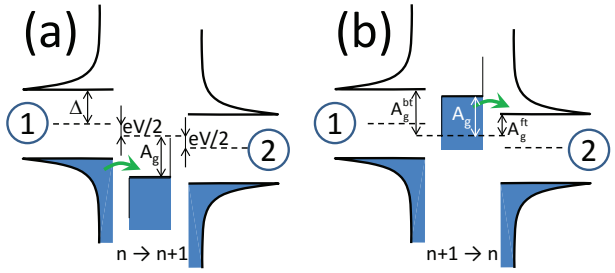

FIG. 2. (Color online) An illustration of the SINIS turnstile operation in the equilibrium regime. Panels show energy diagrams of quasiparticle distributions in superconducting electrodes with a gap Δ and in the normal island for the two stages of the turnstile operation. The two positions $\mu = \mp A_g$ of the island chemical potential, shown by solid black lines, correspond to (a) injection and (b) ejection stages, respectively. The filled (empty) states are shown by blue (white) color, while the electrodes are numbered by 1 and 2 in the circles. Both in the island and in electrodes, the electronic distributions are zero-temperature Fermi distributions. The electrode chemical potentials are shifted by a bias voltage V and are shown by horizontal dashed lines. The main tunneling process of injection (ejection) is shown by the green arrow.

trode, panel (b). This results in a quantized average current $\langle I\rangle = ef$, with $e > 0$ being the elementary charge. In the present paper, we study how the non-equilibrium electron distribution on the island affects the device operation.

The paper is organized as follows. In Sec. II we formulate the theoretical model and write the main equations describing the electron dynamics in the turnstile. Sec. III qualitatively explains the main ideas and the results of the paper. In Sec. IV we study the most interesting regime of the turnstile operation, when the drive is not too slow, and estimate the relevant experimental parameters. In Sec. V, we show that in the opposite case (slow drive) the turnstile errors are very large, so this regime is not interesting. In the last section, we summarize our results.

II. THE MODEL

We assume the single-electron energy levels on the normal island to be randomly distributed with the mean level spacing $\delta = [\nu_{\mathcal{N}}(0)\mathcal{V}]^{-1}$, where $\nu_{\mathcal{N}}(0)$ and $\mathcal{V}$ are the density of states (DOS) per spin projection and the island volume, respectively. Depending on the island size, δ can be large or small compared to other energy scales of the problem. Turnstile devices based both on large[30] and small[32] islands have been realized. Here we focus on the limit of large islands (small δ). We also restrict ourselves to the situation without any external magnetic field, so each level is doubly degenerate with respect to the spin. Tunnel coupling to the electrodes broadens the single-particle levels. Characterizing each tunnel junction $j = 1, 2$ by the conductance G_j it has when the electrode is in the normal state (see Fig. 1), we can relate the average level broadening $\gamma_1 + \gamma_2$ ($2\gamma_j$ being the average escape rate from a single level on the island to the jth electrode in the normal state) to the conductances as $G_j = 2e^2\gamma_j/\delta$, where the factor of 2 keeps track of the spin degeneracy and we set the Planck constant $\hbar = 1$. We assume the tunnel coupling to be weak, $\gamma_j \ll \delta$, to ensure strong Coulomb blockade.[33]

Besides the single-particle contribution to the electronic energy of the island, we include the Coulomb electrostatic contribution. It is determined by the total charge $Q = -ne$ on the island, where n is the total number of the excess electrons there. In addition, one can control the electrostatic energy by applying a voltage V_g to the gate electrode (see Fig. 1). We write the Coulomb energy as $E_n = E_C(n^2 - 2nn_g)$, where the charging energy $E_C = e^2/2C_\Sigma$ is governed by the island total capacitance $C_\Sigma = C_1 + C_2 + C_g$ being the sum of the capacitances to each of the electrodes C_j, $j = 1, 2$, as well as of the capacitance to the gate electrode C_g, and $n_g \equiv C_gV_g/e$. Here we neglect the effects of overheating of S leads due to the success of the QP reduction mentioned in the introduction and assume the electrodes to be in thermal equilibrium at temperature $T \ll \Delta$ small compared to the superconducting gap Δ, and at different chemical potentials $-eV_j$ determined by the applied constant bias voltage V. For simplicity we consider a symmetric device with $C_1 = C_2$, $G_1 = G_2$, $\gamma_1 = \gamma_2 = \gamma$, and $-V_1 = V_2 = V/2 > 0$.

The electronic state of the island is specified by the total electron number n (always an integer), and by the occupations of all single-electron levels. In the statistical description, one works with the probability p_n to have n excess electrons, and with the conditional occupation probability $\mathcal{F}_n(\epsilon)$ of a single-particle state with energy ϵ and a given spin, provided that the island has exactly n excess electrons. They are subject to the constraints $\sum_n p_n = 1$ and

$$\frac{2}{\delta}\int [\mathcal{F}_n(\epsilon) - \theta(-\epsilon)]\, d\epsilon = n\ . \tag{1}$$

As any fermionic distribution function, $\mathcal{F}_n(\epsilon)$ has the limiting values $\mathcal{F}_n(\epsilon \to \pm\infty) = 0, 1$.

We assume the island to be in the strong Coulomb blockade regime, which occurs when $T \ll E_C$ and $\gamma \ll \delta$. Then, if the gate voltage varies within the interval $0 < n_g < 1$, p_n is dominated by at most two values of n close to the minimum of E_n, $n = 0, 1$. As mentioned before we assume the island to be large enough, so that $E_C, eV, \Delta \gg \delta$. Then, many single-particle levels can participate in the transport, so a change of n by 1 translates into a very small change of the occupation probability of each individual level and into a change of the chemical potential by a small amount $\sim \delta$. As a result, one can neglect the difference between the distribution functions $\mathcal{F}_0(\epsilon)$, $\mathcal{F}_1(\epsilon)$, and their average $\mathcal{F}(\epsilon) \equiv p_0\mathcal{F}_0(\epsilon) + p_1\mathcal{F}_1(\epsilon)$ at any given ϵ (see Appendix A). Under the above con-

ditions, one can write a closed set of rate equations for p_n and $\mathcal{F}(\epsilon)$, as it was done in Refs. 34 and 35:

$$\dot{p}_1 = -\dot{p}_0 = \sum_j \frac{2\gamma}{\delta}\left[p_0\, w_+(U_j) - p_1\, w_-(U_j)\right], \tag{2a}$$

$$w_+(U_j) \equiv \int d\epsilon\, n_S(\epsilon)\, \mathcal{F}_T(\epsilon)\left[1-\mathcal{F}(\epsilon-U_j)\right], \tag{2b}$$

$$w_-(U_j) \equiv \int d\epsilon\, n_S(\epsilon)\, \left[1-\mathcal{F}_T(\epsilon)\right]\mathcal{F}(\epsilon-U_j)\ , \tag{2c}$$

$$\begin{aligned}\dot{\mathcal{F}}(\epsilon,t) = {}& \gamma p_0\left[1-\mathcal{F}(\epsilon,t)\right]\sum_j n_S(\epsilon+U_j)\,\mathcal{F}_T(\epsilon+U_j) - \\ & - \gamma p_1 \mathcal{F}(\epsilon,t)\sum_j n_S(\epsilon+U_j)\left[1-\mathcal{F}_T(\epsilon+U_j)\right] + \\ & + \mathrm{St}[\mathcal{F}](\epsilon)\ ,\end{aligned} \tag{3}$$

where the dot denotes the time derivative. Here we introduced $n_S(\epsilon) = \left|\mathrm{Re}\left(\epsilon/\sqrt{\epsilon^2-\Delta^2}\right)\right|$, the quasiparticle DOS in the superconducting electrodes normalized to its normal-state value, and $U_j \equiv \mu + eV_j$ is the change of electrostatic energy due to electron tunneling into the island from the jth electrode with $\mu \equiv E_{n+1} - E_n = 2E_C(n+1/2-n_g)$ playing the role of the chemical potential of the island. $\mathcal{F}_T(\epsilon) \equiv 1/(1+e^{\epsilon/T})$ is the Fermi-Dirac distribution with the bath temperature T.

The last term in Eq. (3), $\mathrm{St}[\mathcal{F}](\epsilon)$, is the collision integral which describes relaxation of the electronic energy distribution towards thermal equilibrium. We consider two relaxation mechanisms, electron-electron and electron-phonon collisions on the island (see, e. g., Ref. 1 for a review),

$$\mathrm{St}[\mathcal{F}](\epsilon) = \mathrm{St}_{ee}[\mathcal{F}](\epsilon) + \mathrm{St}_{eph}[\mathcal{F}](\epsilon). \tag{4a}$$

We describe both in the τ-approximation:

$$\mathrm{St}_{ee}[\mathcal{F}](\epsilon) = \frac{\mathcal{F}_{T_e}(\epsilon) - \mathcal{F}(\epsilon)}{\tau_{ee}}, \tag{4b}$$

$$\mathrm{St}_{eph}[\mathcal{F}](\epsilon) = \frac{\mathcal{F}_{T}(\epsilon) - \mathcal{F}(\epsilon)}{\tau_{eph}}. \tag{4c}$$

Here $\mathcal{F}_{T_e}(\epsilon) = 1/(1+e^{\epsilon/T_e})$ is the Fermi-Dirac distribution with a certain temperature T_e, chosen so that the total energy of the limiting equilibrium distribution $\mathcal{F}_{T_e}(\epsilon)$ matches that in the distribution $\mathcal{F}(\epsilon)$:

$$\frac{2}{\delta}\int \epsilon\left[\mathcal{F}_{T_e}(\epsilon) - \theta(-\epsilon)\right]d\epsilon = \frac{2}{\delta}\int \epsilon\left[\mathcal{F}(\epsilon) - \theta(-\epsilon)\right]d\epsilon\ , \tag{5}$$

where the left-hand side is equal to $\pi^2 T_e^2/(3\delta)$. This ensures that $\mathrm{St}_{ee}[\mathcal{F}](\epsilon)$ conserves the total electronic energy.[36] The electron-phonon processes do not conserve the electronic energy and drive the electronic distribution towards $\mathcal{F}_T(\epsilon)$.

The two relaxation times τ_{ee} and τ_{eph} may depend on electronic temperature T_e, but not on the energy ϵ (such dependence would lead to violation of particle and energy conservation). For τ_{ee}, we assume the temperature dependence corresponding to the zero-dimensional limit:[37,38]

$$\frac{1}{\tau_{ee}} = \delta\,\frac{T_e^2}{E_{\mathrm{Th}}^2}, \tag{6}$$

where E_{Th} is the Thouless energy of the island, defined by the order of magnitude as the inverse of the time required for an electron to travel across the island, thus randomizing its motion due to scattering off impurities or the dot boundaries, $E_{\mathrm{Th}} \sim \min\{v_F/L, D/L^2\}$, where $L \sim \mathcal{V}^{1/3}$ is the typical island size, v_F is the Fermi velocity, and D is the electron diffusion coefficient. In Eq. (6), we omitted the numerical prefactor which is determined by the island shape.

As for the temperature dependence of τ_{eph}, it can be conveniently determined by considering the total power W transferred to phonons from electrons whose distribution $\mathcal{F}_{T_e}(\epsilon)$ is thermal, but with a temperature T_e different from the phonon temperature T. It is related to the electron-phonon collision integral as

$$W = \frac{2}{\delta}\int \epsilon\,\mathrm{St}_{eph}[\mathcal{F}_{T_e}](\epsilon)\,d\epsilon. \tag{7}$$

For this cooling power, a variety of expressions is available in the literature, which were derived microscopically in different regimes determined by the system dimensionality, the shape of the Fermi surface, the relation between the phonon wavelength, island size, and the electron mean free path.[39–44] All these expressions can be represented in the form

$$W = \frac{\pi^2}{3\delta}\,\frac{T_e^\alpha - T^\alpha}{T_{eph}^{\alpha-3}}, \tag{8}$$

with some power α between 4 and 6, and with T_{eph} parameterizing the electron-phonon coupling strength. The proportionality of the cooling power to the island volume $\mathcal{V}$ is ensured by the factor $1/\delta = \nu_{\mathcal{N}}(0)\mathcal{V}$ in Eq. (8). Strictly speaking, it is impossible to obtain an expression of the form (8) from Eq. (7) in the τ approximation (4c) with an energy-independent τ_{eph}. Still, if we use the following model dependence:

$$\frac{1}{\tau_{eph}} = \frac{\max\{T^{\alpha-2}, T_e^{\alpha-2}\}}{T_{eph}^{\alpha-3}}, \tag{9}$$

Eq. (8) matches expression (7) when T_e and T are strongly different. It gives a wrong numerical coefficient in W when $T_e \approx T$, but the τ approximation is valid only qualitatively anyway. In the subsequent numerical calculations, we take $\alpha = 5$, so that Eq. (8) can be equivalently represented in the form $W = \Sigma\mathcal{V}\,(T_e^5 - T^5)$, where Σ is a material constant.[1]

The specific observable we are interested in, is the steady-state period-averaged current $\langle I\rangle$ from the second

to the first electrode. Due to the charge conservation it can be calculated in any of the contacts, say, $j = 2$:

$$\langle I\rangle = e\,\frac{2\gamma}{\delta}\int\limits_0^{\mathcal{T}}\frac{dt}{\mathcal{T}}\Big[p_1(t)\,w_-(U_2) - p_0(t)\,w_+(U_2)\Big]. \quad (10)$$

III. QUALITATIVE DISCUSSION

To achieve the turnstile operation, the gate voltage is driven periodically with frequency f, which leads to a time dependence of $\mu(t)$ via $n_g(t)$. For simplicity we consider a symmetric square drive shape,

$$\mu(t) = \begin{cases} -A_g, & 0 < t < \mathcal{T}/2, \\ A_g, & \mathcal{T}/2 < t < \mathcal{T}, \end{cases} \quad (11)$$

where $\mathcal{T} = 1/f$ and A_g are the drive period and amplitude, respectively.

The main idea of the electron turnstile[30] is to charge the island by transferring one electron from the first electrode during the first half-period (injection stage), so that $p_1(\mathcal{T}/2) \to 1$, and to discharge it through the second electrode in the second half-period, $p_1(\mathcal{T}) = p_1(0) \to 0$ (ejection stage). Ideally, this should lead to a quantized value of the period-averaged current through the device $\langle I\rangle = ef$. Successful turnstile operation implies that the total charge relaxation rate,

$$\Gamma = \sum_j \frac{2\gamma}{\delta}\left[w_+(U_j) + w_-(U_j)\right]\ , \quad (12)$$

well exceeds the drive frequency, $\Gamma \gg f$. The smallness of $\delta \ll E_C, \Delta, eV$ which enabled us to neglect n-dependence of $\mathcal{F}_n(\epsilon)$ also leads to separation between the relaxation time scales of p_n and $\mathcal{F}(\epsilon)$. Namely, the typical relaxation rate of the distribution function $\mathcal{F}(\epsilon)$ at a given energy due to tunneling is $\Gamma_{\mathcal{F}} \lesssim \gamma$ (an electron must enter or leave a given level), while for p_n the typical rate is $\Gamma \sim \gamma(eV/\delta) \gg \Gamma_{\mathcal{F}}$, as an electron entering any of $\sim eV/\delta \gg 1$ levels is sufficient. If, in addition, $\Gamma_{\mathcal{F}} \ll f$, then one can solve rate equations (2) assuming $\mathcal{F}(\epsilon)$ to be fixed and average Eq. (3) over the relaxation time of p_n or over the drive period. In the opposite case one can neglect the deviation of p_n from the stationary solution (see Sec. V).

For the amplitude below the so-called forward-tunneling threshold $A_g^{\rm ft} = \Delta - eV/2$ (we always assume $eV < 2\Delta$) the tunneling rates $w_\pm(U_j)$ are exponentially small. Note that at finite bath temperatures T one can still work in this regime at $A_g \simeq A_g^{\rm ft} - T$. This leads to a refrigerating effect on the normal island which overheats superconducting electrodes. In the following, we consider the amplitudes $A_g > A_g^{\rm ft}$, to have a measurable turnstile current and to avoid overheating of the leads. Still, several processes can lead to a deviation of $\langle I\rangle$ from its ideal value ef. Neglecting all high order processes in the tunneling rates (such as cotunneling, Andreev tunneling, and Cooper pair-electron tunneling)[45] and focusing on the sequential tunneling contributions, we can separate four types of errors related to non-equilibrium effects both in the island and in the superconducting leads:

$$\langle I\rangle = ef(1-2P_{\rm mt})(1-2P_\infty)\,(1-2P_{\rm bt}) + I_{\rm leak}. \quad (13)$$

Here $P_{\rm mt}$ stands for the probability of missed tunneling events if the inequality $\Gamma \gg f$ is not strongly satisfied, so that at too large f electrons do not have enough time to tunnel into (out of) the island during the corresponding half-period. The factor $1 - 2P_\infty$ relates to the Pauli blocking and differs from unity if a finite population of quasiparticles (often non-equilibrium) is present in the leads. The third factor $1 - 2P_{\rm bt}$ in Eq. (13) is due to a combination of back-tunneling processes and drive-dependent leakage which produce tunneling events through the "wrong" junctions: through the first (second) one on the ejection (injection) stage. Finally, the leakage current $I_{\rm leak}$ is present even without drive ($A_g = 0$) and is due to quasiparticles which can tunnel through the device at any time and increase the total current. Typically, $I_{\rm leak}$ is independent of the drive frequency.

The standard picture of the SINIS turnstile operation assumes the electrons both on the island and in the leads to be in equilibrium with the bath, whose temperature T is sufficiently low. This ensures that the density of quasiparticle excitations is negligible, so that the quasiparticle leakage rate is small compared to the drive frequency. Then all error contributions are small. For this equilibrium assumption to be valid, the electron-phonon relaxation time τ_{eph}, must be short enough, $\Gamma_{\mathcal{F}}\tau_{eph} \ll 1$, where $\Gamma_{\mathcal{F}}$ is the typical relaxation rate for the distribution function $\mathcal{F}(\epsilon)$ at a given energy due to the tunneling terms in the kinetic equation (3). In this equilibrium regime, the period-averaged current $\langle I\rangle$ is quantized when the gate amplitude A_g lies in the interval $A_g^{\rm ft} < A_g < A_g^{\rm bt}$ between the forward and backward tunneling thresholds, $A_g^{\rm ft,bt} = \Delta \mp eV/2$ (see Fig. 2(b) for the energy diagram). For $A_g > A_g^{\rm bt}$, the probability $P_{\rm bt}$ of tunneling to the wrong junction becomes of order of unity.

In this work, we investigate the turnstile operation at $\Gamma_{\mathcal{F}}\tau_{eph} \gtrsim 1$, i. e., beyond the equilibrium limit, and demonstrate that even in this case there is a certain range of parameters where the SINIS SET can still work as an electronic turnstile. Specifically, beyond the equilibrium limit we identify three regimes with different behavior of the electron distribution function $\mathcal{F}(\epsilon, t)$ in the normal island.

(i) In the quasiequilibrium regime (see the energy diagram Fig. 3(b) and the light green area close to the origin in Fig. 4), $\Gamma_{\mathcal{F}} \ll f, 1/\tau_{ee}$, the distribution function $\mathcal{F}(\epsilon, t) \approx \mathcal{F}_{T_e}(\epsilon)$ has the Fermi-Dirac form with an effective electronic temperature $T_e \lesssim A_g - A_g^{\rm ft}$, governed by the balance of the heat flows. In this regime the current deviates significantly from ef (except a narrow range,

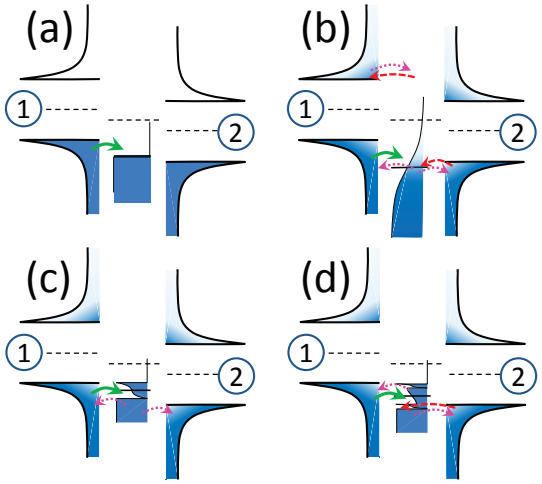

FIG. 3. (Color online) The energy diagrams of a SINIS SET turnstile in the fast drive regimes mentioned in the text, when the drive frequency $f \gg \Gamma_{\mathcal{F}}$, the distribution function relaxation rate $\Gamma_{\mathcal{F}}$ due to tunneling. (a) Equilibrium regime $\Gamma_{\mathcal{F}} \ll \tau_{eph}^{-1}$ at low bath temperature; (b) Quasiequilibrium regime $\tau_{eph}^{-1} \ll \Gamma_{\mathcal{F}} \ll \tau_{ee}^{-1}$ with the long thermal tails of the distribution function $\mathcal{F}(\epsilon)$; (c) and (d) Non-equilibrium regime $\Gamma_{\mathcal{F}} \gg \tau_{ee}^{-1}, \tau_{eph}^{-1}$ for (c) small $A_g < \Delta$ and (d) large $A_g > \Delta$ amplitudes. In all panels the distribution functions in the island shown by blue color correspond to the first half-period (μ is shown by black solid lines). The solid green, dashed red, and dotted purple arrows show the main forward tunneling, backtunneling, and leakage contributions, respectively.

$A_g/A_g^{\rm ft} - 1 \ll 1$, of the parameters near the threshold) due to long thermal tails of $\mathcal{F}_{T_e}(\epsilon)$ as shown by green dash-dotted line in Fig. 5.

(ii) In the fully non-equilibrium regime (see the energy diagrams Fig. 3(c, d) and the blue area on the top of Fig. 4), $1/\tau_{ee} \ll \Gamma_{\mathcal{F}} \ll f$, the tunneling processes form a non-Fermi-Dirac energy profile of $\mathcal{F}(\epsilon)$. This regime is characterized by a wide distribution $\mathcal{F}(\epsilon)$ with sharp jumps at $\epsilon = \pm(A_g - A_g^{\rm ft})$. The sharpness of these jumps, determined by the smearing of the Bardeen-Cooper-Schrieffer (BCS) singularities, ensures good current quantization $\langle I \rangle \simeq ef$ (see Fig. 5) in the gate amplitude interval $A_g^{\rm ft} < A_g < \Delta$ (see Fig. 3(c)), despite a strongly non-equilibrium shape of the distribution function.

(iii) At slow drive (see the dark red area on the right in Fig. 4 and the energy diagram in Fig. 9), $f \ll \Gamma_{\mathcal{F}}$, the distribution function may evolve significantly over the drive period $\mathcal{T} = 1/f$. This regime is characterized by the large leakage current due to the relaxation of $\mathcal{F}(\epsilon, t)$ by electron tunneling processes.

In the next section we focus on the case of the fast drive and study cases (i) and (ii). We will also consider

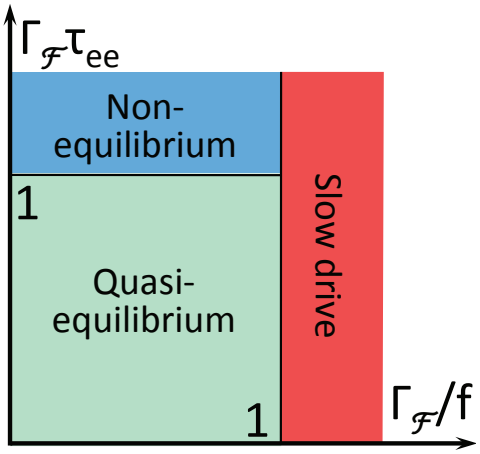

FIG. 4. (Color online) A schematic diagram of different regimes of a SINIS SET turnstile out of equilibrium, $\tau_{eph}^{-1} \ll \Gamma_{\mathcal{F}}$, showing the three regimes discussed in the text.

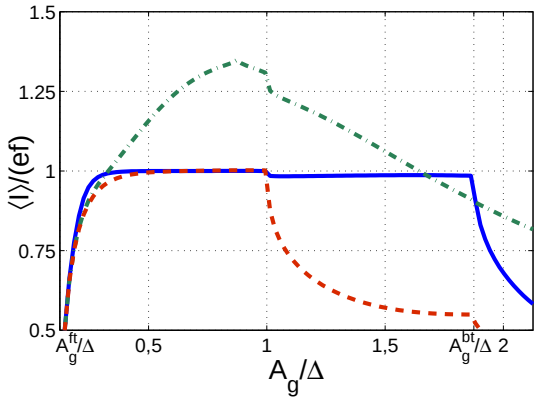

FIG. 5. (Color online) The period-averaged current $\langle I \rangle$ through the SINIS SET versus the drive amplitude A_g/Δ for the equilibrium (blue solid line), quasiequilibrium (green dashed-dotted line) and fully non-equilibrium (red dashed line) regimes discussed in the text, and $eV = 1.75\,\Delta$. The threshold values, $A_g^{\rm ft} = 0.125\,\Delta$ and $A_g^{\rm bt} = 1.875\,\Delta$, are shown explicitly on the horizontal axis. The calculation method and parameter values are discussed below in Sec. IV D and in Fig. 7. The finite widths of the current plateau onsets at small $(A_g - A_g^{\rm ft})/\Delta \lesssim 0.2$ are related to the missed tunneling events due to the regime $\Gamma/f \lesssim 1$.

the equilibrium regime as a reference point. The slow drive limit is studied separately in Sec. V.

IV. FAST DRIVE

Here we take advantage of the assumption $\Gamma_{\mathcal{F}} \ll f$, covering cases (i) and (ii), discussed in the previous section. This assumption enables us to neglect the change in $\mathcal{F}(\epsilon)$ during the period in the first approximation, and

write down the solution for $p_1(t) = 1 - p_0(t)$ as

$$p_1(t < \mathcal{T}/2) = 1 - P_\infty - (1 - 2P_\infty)\,\frac{e^{-\Gamma t}}{1 + e^{-\Gamma\mathcal{T}/2}}\ , \quad (14a)$$

$$p_1(t > \mathcal{T}/2) = P_\infty + (1 - 2P_\infty)\,\frac{e^{-\Gamma(t-\mathcal{T}/2)}}{1 + e^{-\Gamma\mathcal{T}/2}}\ , \quad (14b)$$

where we consider $0 < t < \mathcal{T}$. The quantity P_∞ is specified below. Both Γ and P_∞ depend on $\mathcal{F}(\epsilon)$. For the moment, let us consider $\mathcal{F}(\epsilon)$ as given, it will be determined later from the kinetic equation.

The total charge relaxation rate Γ in Eqs. (14), defined by Eq. (12), is a sum of four terms, $\Gamma = \Gamma_{1+} + \Gamma_{1-} + \Gamma_{2+} + \Gamma_{2-}$, with $\Gamma_{j\pm} = 2\gamma w_\pm(U_j)/\delta$. As long as $\mathcal{F}(\epsilon)$ is assumed to be constant during the period, Γ is also constant. This is the consequence of the electron-hole symmetry of the problem, $\mathcal{F}(\epsilon) = 1 - \mathcal{F}(-\epsilon)$, following from the symmetry of the drive (11). Indeed, each $\Gamma_{j\pm}$ is constant during each half-period, but different on the two half-periods because of the dependence $\mu(t)$, Eq. (11). The symmetry of the latter, however, leads to the relations

$$\Gamma_{1\pm}(0 < t < \mathcal{T}/2) = \Gamma_{2\mp}(\mathcal{T}/2 < t < \mathcal{T}), \quad (15a)$$

$$\Gamma_{2\pm}(0 < t < \mathcal{T}/2) = \Gamma_{1\mp}(\mathcal{T}/2 < t < \mathcal{T}), \quad (15b)$$

so the sum of the four terms is the same on both half-periods. In the following, we will omit the time arguments, referring to the values on the first half-period.

P_∞ in Eqs. (14) represents the limiting probability of having $n = 0$ or 1 excess electrons on the island at the end of the injection or ejection stage, respectively, at long enough times, $\Gamma\mathcal{T} \gg 1$. It is given by

$$P_\infty = \frac{\Gamma_{1-} + \Gamma_{2-}}{\Gamma}. \quad (16a)$$

Out of four terms $\Gamma_{j\pm}$, only Γ_{1+} is large in the equilibrium turnstile operation regime, $A_g^{\rm ft} < A_g < A_g^{\rm bt}$, while the rest are due to residual quasiparticles in the leads and thermal tails of the distribution function in the island, so $P_\infty \ll 1$. Substituting solution (14) into expression (10), we obtain (13) with P_∞ written above and other error contributions given by

$$P_{\rm mt} = \frac{e^{-\Gamma\mathcal{T}/2}}{1 + e^{-\Gamma\mathcal{T}/2}}, \quad (16b)$$

$$P_{\rm bt} = \frac{\Gamma_{2+} + \Gamma_{2-}}{\Gamma}, \quad (16c)$$

$$I_{\rm leak} = e\,\frac{\Gamma_{1+}\Gamma_{2-} - \Gamma_{1-}\Gamma_{2+}}{\Gamma}. \quad (16d)$$

To determine the distribution function $\mathcal{F}(\epsilon)$ which implicitly enters the expressions above, we average Eq. (3) over the period with the help of Eqs. (11) and (14) (as discussed above, the evolution of $\mathcal{F}(\epsilon)$ is slow). Collecting the terms linear in $\mathcal{F}(\epsilon)$ and independent of $\mathcal{F}(\epsilon)$ in the tunneling part of Eq. (3), we can rewrite it identically as

$$\dot{\mathcal{F}}(\epsilon) = \bar{\Gamma}_{\mathcal{F}}(\epsilon)\left[\bar{\mathcal{F}}_{\rm neq}(\epsilon) - \mathcal{F}(\epsilon)\right] + {\rm St}[\mathcal{F}](\epsilon), \quad (17)$$

where $\bar{\Gamma}_{\mathcal{F}}(\epsilon) = \gamma[\bar{w}_{\mathcal{F}}(\epsilon) + \bar{w}_{\mathcal{F}}(-\epsilon)]$ is the period-averaged energy-dependent rate of relaxation towards a certain non-equilibrium distribution $\bar{\mathcal{F}}_{\rm neq}(\epsilon) = \gamma\bar{w}_{\mathcal{F}}(\epsilon)/\bar{\Gamma}_{\mathcal{F}}(\epsilon)$, determined by the tunneling to and from the electrodes. Here we defined

$$\bar{w}_{\mathcal{F}}(\epsilon) = \sum_{\eta=\pm}\left[\left(\frac{1}{2} - \bar{p}\right) n_S^+(A_g + \eta eV/2 - \epsilon) + \bar{p}\, n_S^+(-A_g + \eta eV/2 - \epsilon)\right], \quad (18)$$

$$n_S^+(\epsilon) = n_S(\epsilon)\left[1 - \mathcal{F}_T(\epsilon)\right] \approx n_S(\epsilon)\,\theta(\epsilon)\ , \quad (19)$$

$$\bar{p} = \frac{1}{\mathcal{T}}\int_0^{\mathcal{T}/2} p_1(t)dt = \frac{1}{\mathcal{T}}\int_{\mathcal{T}/2}^{\mathcal{T}} p_0(t)dt = = \frac{1 - P_\infty}{2} - \frac{(1 - 2P_\infty)(1 - 2P_{\rm mt})}{\Gamma\mathcal{T}}\ . \quad (20)$$

The distribution $\bar{\mathcal{F}}_{\rm neq}(\epsilon)$ is very far from the equilibrium one. Although it tends to 0 and 1 in the limits $\epsilon \to \pm\infty$, in the interval $|\epsilon| < A_g - A_g^{\rm ft}$ it has several sharp features, inherited from the BCS singularities in the electrode density of states. $\bar{\mathcal{F}}_{\rm neq}(\epsilon)$ may have different shape, depending on how these singularities, shifted by $\pm A_g$ and/or $\pm eV/2$ are located with respect to each other. In the turnstile regime, $A_g^{\rm ft} < A_g < A_g^{\rm bt}$, it may have two possible shapes which are shown schematically in Fig. 6.

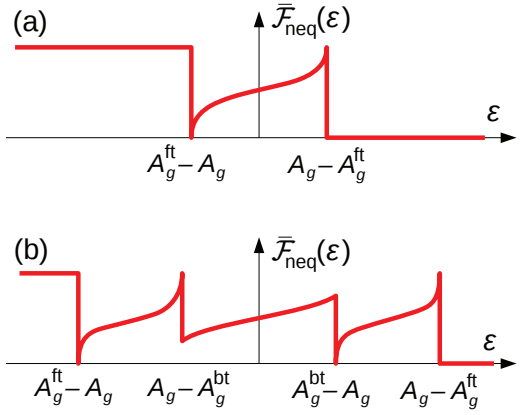

FIG. 6. (Color online) A sketch of the dependence $\bar{\mathcal{F}}_{\rm neq}(\epsilon)$ in the turnstile regime $A_g^{\rm ft} < A_g < A_g^{\rm bt}$ for (a) $A_g < \Delta$ and (b) $A_g > \Delta$.

The relaxation rate $\bar{\Gamma}_{\mathcal{F}}(\epsilon)$ competes with the collision integral which tends to drive the system towards equilibrium. When $\bar{p}$ is close to 1/2, $\bar{\Gamma}_{\mathcal{F}}(\epsilon)$ has quite different values, depending on whether the second term in the expression $\bar{w}_{\mathcal{F}}(\epsilon)$ vanishes or not. Namely, $\bar{\Gamma}_{\mathcal{F}}(\epsilon) \sim \gamma$ for energies $|\epsilon| > A_g + A_g^{\rm ft}$, which corresponds to ejecting electrons from the island into the empty QP bands on

the injection stage, $0 < t < \mathcal{T}/2$, or to electron injection from the deep filled QP states on the ejection stage, $\mathcal{T}/2 < t < \mathcal{T}$. These processes contribute to the errors via the rates Γ_{1-}, Γ_{2-}, which are suppressed when $\mathcal{F}(\epsilon)$ is close to 0 or 1 at $|\epsilon| > A_g + A_g^{\rm ft}$.

In the energy interval $|\epsilon| < A_g + A_g^{\rm ft}$, more important for the turnstile operation, the relaxation rate is smaller, $\bar{\Gamma}_{\mathcal{F}}(\epsilon) \sim \Gamma_{\mathcal{F}}$, which we define as

$$\Gamma_{\mathcal{F}} \equiv \gamma \left(\frac{1}{2} - \bar{p} \right) \approx \frac{\gamma P_\infty}{2} + \frac{f\gamma}{\Gamma}. \tag{21}$$

Here the first contribution γP_∞ is related to the time-independent terms in Eq. (14), while $f\gamma/\Gamma$ is the effective rate associated with fast charge transfer terms in Eq. (14) and originated from the second term in Eq. (20). Because the interval $|\epsilon| < A_g + A_g^{\rm ft}$ is the most important for the turnstile operation, it is $\Gamma_{\mathcal{F}}$ from Eq. (21) that should be used in the validity condition of Eq. (17). In the opposite limit of $\max(\gamma P_\infty, 1/\tau_{ee}) \gg f$, considered in Sec. V, one can neglect the charge relaxation in $p_n(t)$ in the kinetic equation, i.e., in the time-dependent terms in Eq. (14).

In the τ-approximation for the collision integral, Eqs. (4), the steady-state solution of Eq. (17) can be written explicitly:

$$\mathcal{F}(\epsilon) = \frac{\bar{\Gamma}_{\mathcal{F}}(\epsilon)\, \bar{\mathcal{F}}_{\rm neq}(\epsilon) + \mathcal{F}_{T_e}(\epsilon)/\tau_{ee} + \mathcal{F}_T(\epsilon)/\tau_{eph}}{\bar{\Gamma}_{\mathcal{F}}(\epsilon) + 1/\tau_{ee} + 1/\tau_{eph}}\,. \tag{22}$$

Note that due to the symmetry of the drive we have $\bar{\Gamma}_{\mathcal{F}}(\epsilon) = \bar{\Gamma}_{\mathcal{F}}(-\epsilon)$ and $\bar{\mathcal{F}}_{\rm neq}(\epsilon) = 1 - \bar{\mathcal{F}}_{\rm neq}(-\epsilon)$ leading to $\mathcal{F}(\epsilon) = 1 - \mathcal{F}(-\epsilon)$ and $w_-[U] = w_+[-U]$.

Below we consider the limiting cases corresponding to the equilibrium ($\Gamma_{\mathcal{F}} \ll \tau_{eph}^{-1}$), quasiequilibrium ($\tau_{eph}^{-1} \ll \Gamma_{\mathcal{F}} \ll \tau_{ee}^{-1}$) and fully non-equilibrium ($\Gamma_{\mathcal{F}} \gg \tau_{ee}^{-1}$) regimes. Here the typical value of the distribution function relaxation rate $\Gamma_{\mathcal{F}}$ (21) corresponds to the energy interval $|\epsilon| < A_g - A_g^{\rm ft}$ where the major deviations of $\mathcal{F}(\epsilon)$ from the equilibrium one occur. In the following, we show that the plateau $\langle I \rangle = ef$ of the pumping current survives in the equilibrium and, surprisingly, in the fully non-equilibrium regimes, but it is destroyed by the thermal tails of the distribution function in the quasiequilibrium one. Such unusual non-monotonic behavior demonstrates the negative role of the electron-electron relaxation for the turnstile operation, but not of non-equilibrium itself.

A. Equilibrium regime

For reference, we consider first the standard equilibrium regime, when the fast enough electron-phonon relaxation with the rate $\tau_{eph}^{-1} \gg \Gamma_{\mathcal{F}}$ drives the system towards equilibrium with the phonon bath (whatever the relation between τ_{ee} and τ_{eph}). In this case, one can neglect the difference between $\mathcal{F}(\epsilon, t)$ and the equilibrium Fermi distribution $\mathcal{F}_T(\epsilon)$ with the small bath temperature $T \ll \Delta, E_C$. In the turnstile operation regime, $A_g^{\rm ft} < A_g < A_g^{\rm bt}$, only Γ_{1+} is not exponentially small:

$$\Gamma_{1+} = \frac{2\gamma}{\delta} \sqrt{(A_g + eV/2)^2 - \Delta^2}, \tag{23a}$$

$$\Gamma_{2+} = \frac{2\gamma}{\delta} \sqrt{\frac{\pi T \Delta}{2}}\, e^{-(A_g^{\rm bt} - A_g)/T}, \tag{23b}$$

while Γ_{1-} and Γ_{2-} are suppressed by even stronger exponentials $e^{-(A_g + eV/2)/T}$ and $e^{-\max\{\Delta, A_g - eV/2\}/T}$, respectively, not exceeding $e^{-\Delta/T}$ at $A_g > A_g^{\rm ft}$. As a result, both the leakage and the Pauli blocking errors are negligible, and the errors are dominated by the backtunneling,

$$P_{\rm bt} \approx \frac{\Gamma_{2+}}{\Gamma_{1+}} = \sqrt{\frac{(\pi/2) T \Delta}{(A_g + eV/2)^2 - \Delta^2}}\, e^{-(A_g^{\rm bt} - A_g)/T} \tag{24}$$

(we assume the missed tunneling contribution to be well suppressed by the exponential $e^{-\Gamma \mathcal{T}}$). As soon as the drive amplitude exceeds the standard back-tunneling threshold $A_g^{\rm bt} = \Delta + eV/2$, the current $\langle I \rangle$ starts to strongly deviate from the plateau ef.

One may consider corrections to this result due to the deviation of $\mathcal{F}(\epsilon)$ from $\mathcal{F}_T(\epsilon)$, small by the factors $\Gamma_{\mathcal{F}} \tau_{eph}$, τ_{eph}/τ_{ee}. Contributions to the errors from the term with $\mathcal{F}_{T_e}(\epsilon)$ are exponentially small because the electronic temperature T_e, found self-consistently, is close to T (by the same small factors). Contributions originating from $\bar{\mathcal{F}}_{\rm neq}(\epsilon)$ can be calculated analogously to the ones in Sec. IV C; here we note that for $A_g < \Delta$ they are also exponentially small as $e^{-\Delta/T}$, while for $A_g > \Delta$ the smallness is no longer exponential and is guaranteed only by the parameter $\Gamma_{\mathcal{F}} \tau_{eph}$.

B. Quasiequilibrum regime

When $\tau_{eph}^{-1} \ll \Gamma_{\mathcal{F}} \ll \tau_{ee}^{-1}$, one can separate $\mathcal{F}_{T_e}(\epsilon)$ as the main contribution to the distribution function (22),

$$\mathcal{F}(\epsilon) \approx \mathcal{F}_{T_e}(\epsilon) + \tau_{ee} \bar{\Gamma}_{\mathcal{F}}(\epsilon) \left[\bar{\mathcal{F}}_{\rm neq}(\epsilon) - \mathcal{F}_{T_e}(\epsilon) \right] + \\ + \frac{\tau_{ee}}{\tau_{eph}} \left[\mathcal{F}_T(\epsilon) - \mathcal{F}_{T_e}(\epsilon) \right], \tag{25}$$

and naturally rewrite Eq. (5) for the electronic temperature T_e as the heat balance equation:

$$\frac{2}{\delta} \int \epsilon\, \bar{\Gamma}_{\mathcal{F}}(\epsilon) \left[\bar{\mathcal{F}}_{\rm neq}(\epsilon) - \mathcal{F}_{T_e}(\epsilon) \right] d\epsilon = \\ = \frac{2}{\delta} \int \epsilon\, \frac{\mathcal{F}_{T_e}(\epsilon) - \mathcal{F}_T(\epsilon)}{\tau_{eph}}\, d\epsilon. \tag{26}$$

In fact, the right-hand side of this equation is nothing but the total cooling power (7), and in the limit $\Gamma_{\mathcal{F}} \ll \tau_{ee}^{-1}$ this right-hand side can be replaced by the more precise dependence (8). Moreover, one can actually take the limit $\tau_{eph} \to \infty$ and set the right-hand side of Eq. (26) to zero. Even in this case, a finite value of T_e is obtained, which satisfies the following equation:

$$\int \epsilon\, \bar{w}(-\epsilon)\, \mathcal{F}_{T_e}(\epsilon)\, d\epsilon = 0. \tag{27}$$

This equation has a unique solution $T_e \sim A_g - A_g^{\rm ft}$.

Near the forward tunneling threshold, $0 < A_g - A_g^{\rm ft} \ll eV$, the temperature $T_e = (A_g - A_g^{\rm ft})/c_0$, with $c_0 = 0.7233\ldots$, and we can evaluate

$$\Gamma_{1+} = \frac{2\gamma}{\delta} \int\limits_{A_g^{\rm ft}-A_g}^{\infty} n_S^+(\epsilon + A_g + eV/2)\, \mathcal{F}_{T_e}(\epsilon)\, d\epsilon \approx$$
$$\approx c_1 \frac{2\gamma}{\delta} \sqrt{(A_g - A_g^{\rm ft})\Delta}, \qquad (28a)$$
$$\Gamma_{2+} = \frac{2\gamma}{\delta} \int\limits_{A_g^{\rm bt}-A_g}^{\infty} n_S^+(\epsilon + A_g - eV/2)\, \mathcal{F}_{T_e}(\epsilon)\, d\epsilon \approx$$
$$\approx c_2 \frac{2\gamma}{\delta} \sqrt{(A_g - A_g^{\rm ft})\Delta}\, e^{-c_0 eV/(A_g - A_g^{\rm ft})}, \qquad (28b)$$

where the numerical factors are approximately given by $c_1 = 1.3329\ldots$, $c_2 = 6.0751\ldots$. Other rates are suppressed by even stronger exponentials, $\Gamma_{1-,2-} \sim \Gamma_{1+} e^{-c_0(A_g+\Delta\pm eV/2)/(A_g - A_g^{\rm ft})}$.[46] However, away from the threshold, when $A_g - A_g^{\rm ft} \sim eV$, the electronic temperature rapidly increases and so do all errors. Thus, in most of the quasiequilibrium regime, the electron-electron collisions are detrimental for the turnstile operation.

C. Fully non-equilibrium regime

When $\tau_{eph}^{-1}, \tau_{ee}^{-1} \ll \Gamma_{\mathcal{F}}$, the distribution function can be written as

$$\mathcal{F}(\epsilon) = \bar{\mathcal{F}}_{\rm neq}(\epsilon) + \frac{{\rm St}[\bar{\mathcal{F}}_{\rm neq}](\epsilon)}{\bar{\Gamma}_{\mathcal{F}}(\epsilon)} + O\left(\frac{{\rm St}[\bar{\mathcal{F}}_{\rm neq}]^2}{\bar{\Gamma}_{\mathcal{F}}^2}\right). \qquad (29)$$

Let us start by analyzing the main term, $\bar{\mathcal{F}}_{\rm neq}(\epsilon)$, and its contribution to the turnstile errors. In the range $A_g^{\rm ft} < A_g < \Delta$, the distribution $\bar{\mathcal{F}}_{\rm neq}(\epsilon)$ has the shape, shown schematically in Fig. 6(a) and is given by the simple expression,

$$\bar{\mathcal{F}}_{\rm neq}(\epsilon) = \frac{n_S^+(A_g + \frac{eV}{2} - \epsilon)}{n_S^+(A_g + \frac{eV}{2} - \epsilon) + n_S^+(A_g + \frac{eV}{2} + \epsilon)}. \qquad (30)$$

A similar behavior of the distribution function was predicted theoretically for the dc mode of an analogous setup beyond the subgap regime $eV > 2\Delta$ in Ref. 29, as well as for an entirely superconducting device in Ref. 47 This determines the dominant among the four rates $\Gamma_{j\pm}$,

$$\Gamma_{1+} = \frac{2\gamma}{\delta} \int\limits_{\Delta}^{2A_g - \Delta + eV} \frac{n_S(\epsilon)\, n_S(2A_g + eV - \epsilon)}{n_S(\epsilon) + n_S(2A_g + eV - \epsilon)}\, d\epsilon =$$
$$= \frac{2\gamma}{\delta} \sqrt{2(A_g - A_g^{\rm ft})\Delta} \left[\sqrt{2} + \ln(\sqrt{2} - 1)\right] +$$
$$+ \frac{2\gamma}{\delta} O\left((A_g - A_g^{\rm ft})^{3/2}/\sqrt{\Delta}\right), \qquad (31)$$

where we only give an explicit expression near the threshold, $A_g - A_g^{\rm ft} \ll \Delta$ (although the integral can be calculated exactly, the resulting expressions are quite bulky and not very informative). The rest of the rates, $\Gamma_{2+}, \Gamma_{1-}, \Gamma_{2-}$, are all exponentially suppressed as $\propto e^{-\Delta/T}$, where T is the bath temperature, as they are determind by the quasiparticle population in the superconducting electrodes. This happens because at $A_g^{\rm ft} < A_g < \Delta$, the energy range where $\bar{\mathcal{F}}_{\rm neq}(\epsilon - U_j)$ in Eqs. (2b), (2c) for $\Gamma_{2+}, \Gamma_{1-}, \Gamma_{2-}$ is different from 0 or 1, falls inside the superconducting gap in $n_S(\epsilon)$.

The situation changes dramatically at $A_g > \Delta$, when the energy interval of $\bar{\mathcal{F}}_{\rm neq}(\epsilon)$ widens, and a second peak-dip structure appears, as shown in Fig. 6(b). Then, back-tunneling becomes allowed and its rate Γ_{2+} is no longer exponentially small; near the threshold, $0 < A_g - \Delta \ll \Delta, eV$, the rate Γ_{2+} is given by the same expression (31) with the replaced threshold, $A_g^{\rm ft} \to \Delta$. Thus, at $A_g > \Delta$, the turnstile accuracy quickly drops.

We now turn back to the "good" region, $A_g^{\rm ft} < A_g < \Delta$, and study errors originating from the subleading term in Eq. (29). These errors are important as they have no exponential smallness $e^{-\Delta/T}$, in contrast to those originating from the main term. Indeed, the temperature T_e determining the electron-electron part of the collision integral (4b), is not necessarily low. Up to small corrections, T_e can be found from the equation

$$\int \epsilon \left[\bar{\mathcal{F}}_{\rm neq}(\epsilon) - \theta(-\epsilon)\right] d\epsilon = \frac{\pi^2 T_e^2}{6}. \qquad (32)$$

Quite analogously to the quasiequilibrium case, this gives $T_e \sim A_g - A_g^{\rm ft}$. We can give an analytical expression for the main error only near the forward threshold, $0 < A_g - A_g^{\rm ft} \ll eV$:

$$\Gamma_{2+} \approx \frac{c_2'}{(1/2 - \bar{p})\tau_{ee}} \frac{A_g - A_g^{\rm ft}}{\delta}\, e^{-c_0' eV/(A_g - A_g^{\rm ft})}, \qquad (33)$$
$$P_{\rm bt} \approx \frac{c_2' \mathcal{T}}{\tau_{ee}} \frac{A_g - A_g^{\rm ft}}{\delta}\, e^{-c_0' eV/(A_g - A_g^{\rm ft})}, \qquad (34)$$

with the numerical factors $c_0' = 1.52\ldots$, $c_2' = 6.01\ldots$. Here we assumed that the main contribution to $1/2 - \bar{p}$ comes from $1/(\Gamma\mathcal{T})$, rather than from P_∞ [see Eq. (20)].

D. Parameter estimates and crossovers

To illustrate the three regimes, described above, we present in Fig. 7 the dependence of the turnstile current $\langle I\rangle/(ef)$ on the drive amplitude, $(A_g - A_g^{\rm ft})/\Delta$, relative to the threshold value, which is obtained by the direct numerical evaluation of Eq. (13) via Eqs. (16) with the rates $\Gamma_{j\pm}$ evaluated using the distribution function (22).

First, we estimate the possible parameters for each of the cases. Typical frequencies of the turnstile operation are usually limited from above by the missed tunneling events (16b) and the overheating of superconducting leads as $f \lesssim 300$ MHz. Here we consider electrodes

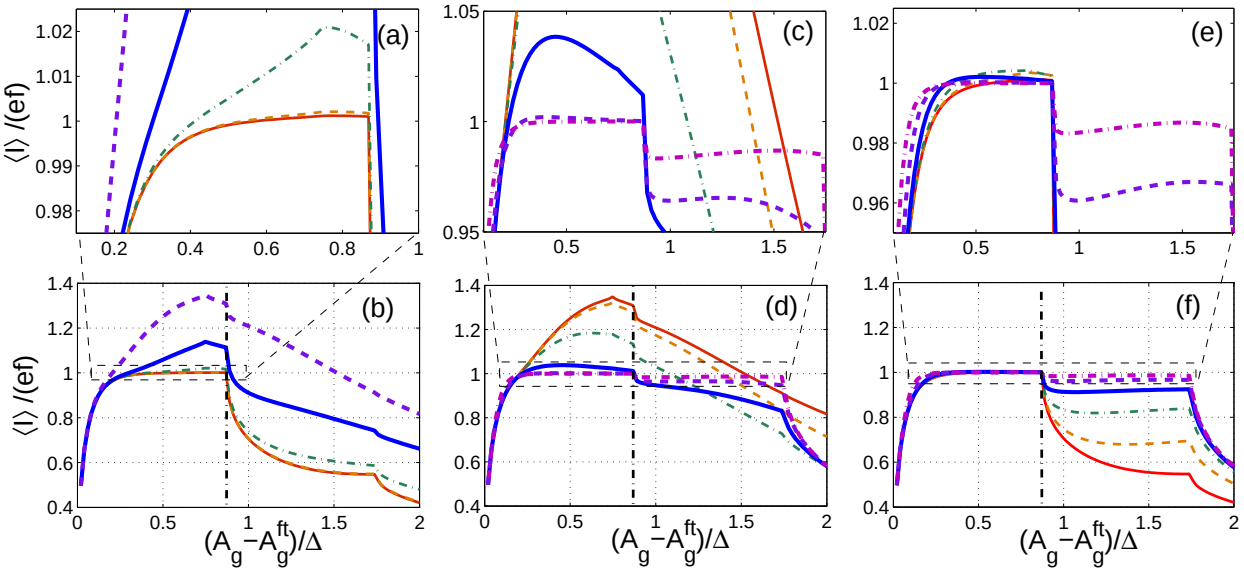

FIG. 7. (Color online) The period-averaged current $\langle I\rangle$ through the SINIS SET versus the drive amplitude $(A_g - A_g^{\rm ft})/\Delta$ relative to the threshold value for the equilibrium (Eq), $\Gamma_{\mathcal F} \ll \tau_{eph}^{-1}$, quasiequilibrium (QEq), $\tau_{eph}^{-1} \ll \Gamma_{\mathcal F} \ll \tau_{ee}^{-1}$, and fully non-equilibrium (NEq), $\tau_{eph}^{-1}, \tau_{ee}^{-1} \ll \Gamma_{\mathcal F}$, regimes and crossovers between them. In panels (a), (c), and (e) we represent zooms of the regions shown by dashed rectangles in panels (b), (d), and (f) near the plateau $\langle I\rangle = ef$. (a), (b) NEq – QEq crossover governed by the decrease of $l_{\rm mfp}$ from 1 (red thin solid) to $2.4\cdot 10^{-2}$ (violet thick dashed-dotted) by a factor $\sqrt{10}$ at each step. This corresponds to the change of the Thouless energy $E_{\rm Th}/\Delta$ from 75 (red thin solid) to 1.8 (violet thick dashed-dotted). We take $\delta/\Delta = 10^{-2}$ keeping $\Gamma_{\mathcal F}$ constant. (c), (d) QEq – Eq crossover governed by the decrease of δ/Δ from 10^{-2} (red thin solid) to 10^{-7} (violet thick dashed-dotted curve) by a factor 10 at each step. We choose $l_{\rm mfp} \propto (\delta/\Delta)^{-1/3}$ and change it from $2.4\cdot 10^{-2}$ up to 1 to keep the Thouless energy constant, $E_{\rm Th}/\Delta = 1.8$. This effectively changes only $\Gamma_{\mathcal F} \simeq f\delta/\Delta$. In all curves $\tau_{ee}^{-1} \gg \Gamma_{\mathcal F}$. (e), (f) NEq – Eq crossover governed by the decrease of δ/Δ from 10^{-2} (red thin solid) to 10^{-7} (violet thick dashed-dotted curve) by a factor 10 at each step. We consider the maximal possible Thouless energy taken at $l_{\rm mfp} = 1$, however, due to δ-dependence of $E_{\rm Th}/\Delta$, it also varies from 75 (red thin solid) to 1.8 (violet thick dashed-dotted). In all panels we considered the island made of AlMn ($T_{eph} = 250$ K, $E_F = 11.7$ eV and $\nu_{\mathcal N}(0) = 1.45\cdot 10^{47}$ J^{-1} m^{-3}) and take $eV = 1.75\Delta$, $f/\Delta = 2\cdot 10^{-3} \simeq 300$ MHz, $\gamma/\delta = 4\cdot 10^{-2} \gg f/\Delta$. In panels (b), (d), and (f) the vertical dashed-dotted line shows the amplitude threshold value $A_g = \Delta$ for the non-equilibrium case. The finite widths of the current plateau onsets at small $(A_g - A_g^{\rm ft})/\Delta \lesssim 0.2$ are related to the missed tunneling events due to the regime $\Gamma/f \lesssim 1$.

made of aluminum and take into account some reduction of the superconducting gap due to the possible usage of quasiparticle traps and/or active cooling taking $\Delta = 1$ K. Then, considering $f = 300$ MHz, we can still neglect the finite QP density in the leads due to a exponentially small prefactor $e^{-\Delta/T}$ and take into account only the second term in (21) giving $\Gamma_{\mathcal F} \sim f\delta/\Delta$. Here and further we assume $A_g, eV \sim \Delta$ and fix the ratio γ/δ to the value $4\cdot 10^{-2}$ ensuring $\Gamma \sim \gamma\Delta/\delta \gg f \simeq 2\cdot 10^{-3}\Delta$.

The parameter T_{eph} governing electron-phonon relaxation rate (9) depends only on the material of the normal island and varies between ~ 60 K for Au and ~ 250 K for AlMn.[1,48] The Thouless energy governing electron-electron relaxation (6) $E_{\rm Th} \sim \min\{v_F/L, D/L^2\} \sim E_F^{2/3}\delta^{1/3} l_{\rm mfp}$ can be expressed in terms of the mean level spacing δ determined by the island size $L \sim \mathcal{V}^{1/3}$, of the Fermi energy $E_F \sim 1-10$ eV (for typical metals) through the Fermi velocity v_F, and of the mean free path ℓ in the island normalized to its size $l_{\rm mfp} = \min\{1, \ell/L\}$.

To achieve the fully non-equilibrium case (ii) one needs both following ratios to be large:

$$\Gamma_{\mathcal F}\tau_{eph} = \frac{f\delta}{\Delta}\frac{T_{eph}^2}{T_e^3} \gg 1\,, \tag{35a}$$

$$\Gamma_{\mathcal F}\tau_{ee} = \frac{f}{\Delta}\frac{E_{\rm Th}^2}{T_e^2} \sim \frac{f}{\Delta}\frac{E_F^{4/3}\delta^{2/3} l_{\rm mfp}^2}{T_e^2} \gg 1\,, \tag{35b}$$

with $T_e \sim A_g - A_g^{\rm ft} \sim \Delta$. To maximize $T_{eph} = 250$ K and $l_{\rm mfp} = 1$ we assume the island to be made of AlMn with a sufficiently low Mn concentration ensuring $\ell > L$, $E_F \simeq 11.7$ eV, and $\nu_{\mathcal N}(0) = 1.45\cdot 10^{47}$ J^{-1} m^{-3}. After this material optimization we are left with the only free parameter δ to make the ratios large. Within the assumption of continuous spectrum $\delta/\Delta \ll 1$ we consider $\delta = 10^{-2}\Delta$ corresponding to the island size $L \sim \mathcal{V}^{1/3} \simeq 50$ nm achievable with existing experimental techniques.[52] This gives $\Gamma_{\mathcal F}\tau_{eph} \sim 100$ and $\Gamma_{\mathcal F}\tau_{ee} \sim 200$ for the typical electronic temperature in this case $T_e \simeq 0.25\Delta$. The corresponding plot of $\langle I\rangle/(ef)$ vs $(A_g - A_g^{\rm ft})/\Delta$ is shown by the red dashed curve in Fig. 5 and by the red thin solid curves in panels (a), (b), (e), (f) of Fig. 7.

By reducing the mean free path $l_{\rm mfp}$ in the island from unity, one enhances the electron-electron relaxation rate keeping the electron-phonon rate intact, so that the system crosses from the fully non-equilibrium case (ii), $\tau_{ee}^{-1}, \tau_{eph}^{-1} \ll \Gamma_{\mathcal{F}}$, to the quasi-equilibrium case (i), $\tau_{eph}^{-1} \ll \Gamma_{\mathcal{F}} \ll \tau_{ee}^{-1}$. This crossover is shown by the curves (from red to violet) in Fig. 7(b) with the zoom near the plateau $\langle I \rangle = ef$ in Fig. 7(a). The parameters used are mentioned in the caption. The representative curves in the quasiequilibrium regime with the parameters $\delta = 10^{-2}\Delta$ and $l_{\rm mfp} = 2.4 \cdot 10^{-2}$ corresponding to $E_{\rm Th}/\Delta = 1.8$ are shown by dash-dotted green line in Fig. 5 and by dashed thick violet and red thin solid lines in panels (a), (b) and (c), (d) of Fig. 7, respectively.

To go further to the equilibrium regime, $\tau_{eph}^{-1} \gg \Gamma_{\mathcal{F}}$, one has to decrease the mean level spacing governing both ratios (35). To keep electron-electron relaxation fixed in Fig. 7(c), (d) we choose $E_{\rm Th}/\Delta = 1.8$ and $l_{\rm mfp} \propto (\delta/\Delta)^{-1/3}$. We decrease δ/Δ down to 10^{-7} where $l_{\rm mfp}$ achieves its maximal value equal to 1. However, as one can see from the solid blue curves in Fig. 5 and in panels (c)–(f) of Fig. 7, even in this regime there is a small step in the plateau close to $A_g = \Delta$ related to the non-equilibrium contribution to the turnstile current.

Finally, we consider the most nontrivial crossover from full non-equilibrium to equilibrium which can be achieved by decreasing the parameter δ/Δ from the maximal considered value 10^{-2} to 10^{-7} [see Fig. 7(e), (f)]. In this case the Thouless energy $E_{\rm Th} \propto (\delta/\Delta)^{1/3}$ also changes due to the fixed value of $l_{\rm mfp} = 1$ needed to suppress electron-electron relaxation during the crossover. Because of this, on some curves close to the non-equilibrium regime (red, orange, green) in the zoom Fig. 7(e) one can see an overshooting more typical for the quasiequilibrium regime.

It is important that the relaxation times τ_{ee}, τ_{eph}, which determine $\mathcal{F}(\epsilon)$ in Eq. (22), depend on the effective electronic temperature, T_e, via Eqs. (6), (9), while T_e itself is determined by $\mathcal{F}(\epsilon)$ via Eq. (5), so T_e has to be found self-consistently. As a result, T_e increases with A_g, and so do the rates $\tau_{ee}^{-1}, \tau_{eph}^{-1}$. Thus, when A_g is changed, the device can switch between different regimes. For example, the green curves in Figs. 7(c)–(f) corresponding to $\delta/\Delta = 10^{-4}$ go from quasiequilibrium (c), (d) or fully-nonequilibrium (e), (f) behavior at small $(A_g - A_g^{\rm ft})/\Delta$ to the equilibrium one at large amplitudes.

V. SLOW DRIVE

Now we consider the slow drive case, $f \ll \Gamma_{\mathcal{F}}$, where $\Gamma_{\mathcal{F}}$ is time-dependent and varies between γ and γP_∞ during each half-period. Thus, we are assuming $f \ll \gamma P_\infty$. Anticipating the results to be derived below, we note that in this case, the leakage current turns out to be always large compared to ef, so the SINIS SET at slow drive cannot be considered as a turnstile anymore.

Using the same assumptions as for the fast drive, $\mathcal{F}_0 = \mathcal{F}_1 \equiv \mathcal{F}(\epsilon, t)$ and $\Gamma \gg \Gamma_{\mathcal{F}}, \tau_{ee}^{-1}, \tau_{eph}^{-1}$, one can write the solutions (14) for the occupation probabilities $p_n(t)$ and substitute them into Eq. (3), which can be written in the form of Eq. (17),

$$\dot{\mathcal{F}}(\epsilon) = \Gamma_{\mathcal{F}}(\epsilon, t)\left[\mathcal{F}_{\rm neq}(\epsilon, t) - \mathcal{F}(\epsilon)\right] + \\ + \frac{\mathcal{F}_{T_e(t)}(\epsilon) - \mathcal{F}(\epsilon)}{\tau_{ee}} + \frac{\mathcal{F}_T(\epsilon) - \mathcal{F}(\epsilon)}{\tau_{eph}}, \qquad (36)$$

with the time-dependent functions

$$\Gamma_{\mathcal{F}}(\epsilon, t) = \gamma \sum_{\eta=\pm} [1 - p_1(t)]\, n_S^+\left(-\mu(t) + \eta\tfrac{eV}{2} - \epsilon\right) + \\ + \gamma \sum_{\eta=\pm} p_1(t)\, n_S^+\left(\mu(t) - \eta\tfrac{eV}{2} + \epsilon\right), \qquad (37)$$

$$\mathcal{F}_{\rm neq}(\epsilon, t) = \gamma \frac{1 - p_1(t)}{\Gamma_{\mathcal{F}}(\epsilon, t)} \sum_{\eta=\pm} n_S^+\left(-\mu(t) + \eta\tfrac{eV}{2} - \epsilon\right). \qquad (38)$$

Here $\mu(t)$ is given by (11). Note that τ_{ee}, τ_{eph} are also time-dependent, as they depend on the electronic temperature $T_e(t)$. Due to the condition $\Gamma \gg \Gamma_{\mathcal{F}} \gg f$, leakage will be dominated by the longest part of each half-period when $p_1(t)$ has reached its stationary value ($1 - P_\infty$ and P_∞ on the injection and the ejection stage, respectively). Thus, we neglect all terms, proportional to $e^{-\Gamma t}$.

As we saw in Sec. IV, the most interesting is the non-equilibrium regime, $\Gamma_{\mathcal{F}} \gg f, \tau_{eph}^{-1}, \tau_{ee}^{-1}$, when the relaxation of the distribution function $\mathcal{F}(\epsilon)$ is dominated by tunneling. For the fast drive, turnstile errors were small in this regime; now we will show that for the slow drive this is no longer the case. Due to the symmetry of the drive, $\mu(t + \mathcal{T}/2) = -\mu(t)$, and of the resulting distribution function, $\mathcal{F}(\epsilon, t + \mathcal{T}/2) = 1 - \mathcal{F}(-\epsilon, t)$, we consider the relaxation of $\mathcal{F}(\epsilon, t)$ to its stationary value only in the first half-period $0 < t < \mathcal{T}/2$ with $\mu(0 < t < \mathcal{T}/2) = -A_g$. One can identify three energy intervals: (I) $\epsilon > A_g + A_g^{\rm ft}$ where $\mathcal{F}(\epsilon)$ relaxes to a small value $\mathcal{F}_{\rm neq} \lesssim P_\infty e^{-\Delta/T}$ with the rate $\Gamma_{\mathcal{F}} \sim \gamma$; (II) $A_g - A_g^{\rm ft} < \epsilon < A_g + A_g^{\rm ft}$ where $\Gamma_{\mathcal{F}} = 0$, the distribution function does not relax, and its value is determined by the relaxation during the other half-period; (III) $\epsilon < A_g - A_g^{\rm ft}$ where $\mathcal{F}(\epsilon)$ relaxes with the rate $\Gamma_{\mathcal{F}} \sim \gamma P_\infty$ to some nontrivial function considered below [see Fig. 8(a)]. Note that unlike the fast drive case, we need a more accurate expression for the function

$$n_S^+(\epsilon) = n_S(\epsilon)\left[1 - \mathcal{F}_T(\epsilon)\right] \approx \\ \approx n_S(\epsilon)\left[\theta(\epsilon - \Delta) + \theta(-\Delta - \epsilon)\, e^{\epsilon/T}\right], \qquad (39)$$

including terms of order of $P_\infty \lesssim e^{-\Delta/T}$.

In the first interval, we denote $y = \epsilon - (A_g + A_g^{\rm ft}) > 0$

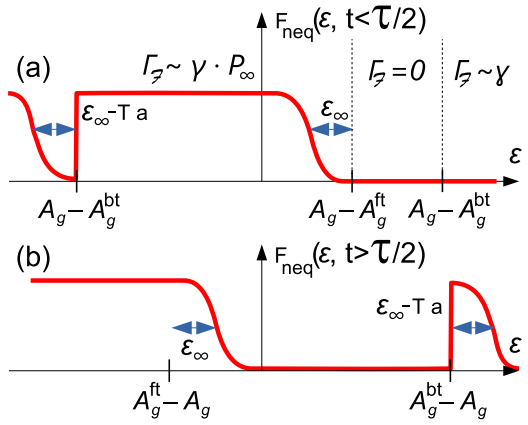

FIG. 8. (Color online) A sketch of $\mathcal{F}_{\rm neq}(\epsilon)$ in the turnstile regime $A_g^{\rm ft} < A_g < A_g^{\rm bt}$ for a slow drive out of equilibrium $f, \tau_{eph}^{-1}, \tau_{ee}^{-1} \ll \Gamma_{\mathcal{F}}$ at (a) the first and (b) second halves of the period. In panel (a) the approximate values of the distribution function relaxation rate $\Gamma_{\mathcal{F}}$ due to tunneling are shown for the energy intervals (i-iii) mentioned in the text.

and obtain

$$\Gamma_{\mathcal{F}}(\epsilon) = \frac{\gamma}{2}\, n_S(\Delta + y)\left[1 + P_\infty e^{-(\Delta+y)/T}\right] + \\ + \frac{\gamma}{2}\,\theta(\Delta - eV + y)\, n_S(\Delta - eV + y) \times \\ \times \left[1 + P_\infty e^{-(\Delta - eV + y)/T}\right] \sim \gamma, \qquad (40)$$

while

$$\Gamma_{\mathcal{F}}(\epsilon)\,\mathcal{F}_{\rm neq}(\epsilon) = \frac{\gamma}{2}\, n_S(\Delta + y) P_\infty e^{-(\Delta+y)/T} + \\ + \frac{\gamma}{2}\,\theta(\Delta - eV + y)\, n_S(\Delta - eV + y) \times \\ \times P_\infty e^{-(\Delta - eV + y)/T} \lesssim \gamma e^{-2\Delta/T}. \qquad (41)$$

As we neglected the contributions of the order of $e^{-2\Delta/T}$ in (39), we should set $\mathcal{F}_{\rm neq}(\epsilon > A_g + A_g^{\rm ft}) = 0$ within this approximation in order to be consistent.

In the third interval, we denote $x = A_g - A_g^{\rm ft} - \epsilon > 0$ and obtain that the rate

$$\Gamma_{\mathcal{F}}(\epsilon) = \frac{\gamma}{2}\, n_S(\Delta + x)\left[P_\infty + e^{-(\Delta+x)/T}\right] + \\ + \frac{\gamma}{2}\,\theta(\Delta - eV + x)\, n_S(\Delta - eV + x) \times \\ \times \left[P_\infty + e^{-(\Delta - eV + x)/T}\right] \sim \\ \sim \gamma \max\{P_\infty, e^{-\Delta/T}\}, \qquad (42)$$

and its product with the distribution function,

$$\Gamma_{\mathcal{F}}(\epsilon)\,\mathcal{F}_{\rm neq}(\epsilon) = \frac{\gamma}{2}\, n_S(\Delta + x)\, P_\infty + \\ + \frac{\gamma}{2}\,\theta(\Delta - eV + x)\, n_S(\Delta - eV + x) P_\infty \\ \sim \Gamma_{\mathcal{F}}(\epsilon), \qquad (43)$$

are of the same order. Parameterizing $P_\infty = e^{-(\Delta+\epsilon_\infty)/T}$ by a positive energy $\epsilon_\infty > 0$, we can write the resulting distribution function in the form of a double Fermi function (see Figs. 8, 9)

$$\mathcal{F}_{\rm neq}(\epsilon) = \begin{cases} \mathcal{F}_T(\epsilon_\infty - x), & x < eV, \\ \mathcal{F}_T(\epsilon_\infty + eV - x - Ta), & x > eV. \end{cases} \qquad (44)$$

Here $a = \ln[1 + n_S(\Delta + x)/n_S(\Delta - eV + x)]$ is bounded by $1 < a < 2$, and we neglected exponentially small factors $e^{-(eV-\epsilon_\infty)/T}$ for $eV - \epsilon_\infty \gg T > 0$. For the case $\epsilon_\infty - eV \gg T > 0$ function (44) becomes the Fermi-Dirac function $\mathcal{F}_{\rm neq}(\epsilon) = \mathcal{F}_T(\epsilon_\infty + eV - x - Ta)$ with zero values at $x < eV$.

By definition, P_∞ is determined by the distribution function itself via Eqs. (16a), (2b), (2c). Only the values of $\mathcal{F}(\epsilon)$ in the intervals (I) and (III) enter the integrals in Eqs. (2b), (2c), and when one substitutes there $\mathcal{F}(\epsilon)$ found above, Eq. (16a) becomes an identity. Thus, to find P_∞ or ϵ_∞, it is necessary to use constraint (1),

$$\frac{2}{\delta}\int [\mathcal{F}(\epsilon) - \theta(-\epsilon)]\, d\epsilon = p_1. \qquad (45)$$

This equation is sensitive to $\mathcal{F}(\epsilon)$ in the nonrelaxing interval (II), determined by the relaxation on the previous half-period. It is important that for $A_g > A_g^{\rm ft}$, interval (II) maps on interval (III) of the previous half-period, so there is no uncertainty in $\mathcal{F}(\epsilon)$. The solution for ϵ_∞ depends on the relation between A_g, eV, and Δ, and the allowed region $A_g > \Delta - eV/2$, $0 < eV < 2\Delta$ of the (eV, A_g) plane splits into 7 subregions. We study in detail the simplest case of $\mathcal{F}(A_g - A_g^{\rm ft} < \epsilon < A_g + A_g^{\rm ft}) = 0$, realized when either $\Delta + eV/6 < A_g < \Delta + 3eV/2$ or $\Delta - eV/2 < A_g < eV/2$. For other arrangements of A_g, eV, and Δ, the distribution has a different shape, but the results for the leakage current are qualitatively similar to the one obtained below, so we do not give details for these cases.

In the simplest case of $\mathcal{F}(A_g - A_g^{\rm ft} < \epsilon < A_g + A_g^{\rm ft}) = 0$, we obtain $\epsilon_\infty \approx (A_g - A_g^{\rm ft})/2$ which is just the conservation of the chemical potential (the number of filled states, $(A_g - A_g^{\rm ft} - \epsilon_\infty)/\delta$, above the Fermi energy should be equal to the number of empty states, $\sim \epsilon_\infty/\delta$, below). The corresponding distribution is shown in Figs. 8 and 9. The relaxation bottleneck is the discharging process with the rates $\Gamma_{j-} \sim \gamma n_{qp} e^{-(|\epsilon| - \Delta - eV_j)}[1 - \mathcal{F}(\epsilon)]$ occurring in the first half-period due to a small density of hole-like quasiparticles $n_{qp} \sim e^{-\Delta/T}$ with a narrow thermal distribution, $e^{-(|\epsilon| - \Delta - eV_j)}$, concentrated near the quasiparticle band edge, $-\Delta - eV_j$. The charging process is suppressed by the factor $p_0(t) = P_\infty$ of the small probability for the island to be discharged. The balance between the charging rate, $P_\infty \Gamma_{1+}$, with a weak energy dependence, and the discharging rates Γ_{j-} in both electrodes with the thermal exponential energy dependence $e^{-(|\epsilon| - \Delta - eV_j)}$ formes the double Fermi distribution $\mathcal{F}(\epsilon)$. The effective chemical potentials of these Fermi functions are shifted from the gap edges to nearly the same value

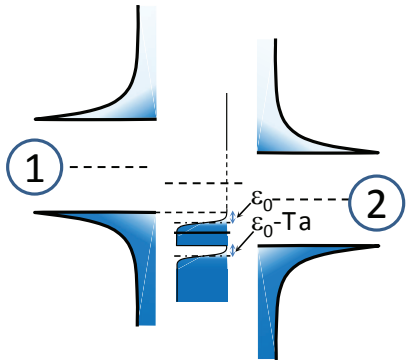

FIG. 9. (Color online) The energy diagram of a SINIS SET turnstile in the regimes of slow drive out of equilibrium $f, \tau_{eph}^{-1} \ll \Gamma_{\mathcal{F}}$. The distribution function in the island shown by blue color corresponds to the first half-period. The corresponding chemical potential is shown by the black solid line. The shifts of the effective chemical potentials of the Fermi functions relatively to the edges of the superconducting DOSes of the leads are shown explicitly.

$\simeq \epsilon_\infty$ which conserves the overall chemical potential of $\mathcal{F}_{\rm neq}$ and determines P_∞ via Eq. (45).

It is quite easy to see now that the described relaxation dynamics leads to a large leakage current. Indeed, using the symmetry $\mathcal{F}(\epsilon, t+\mathcal{T}/2) = 1 - \mathcal{F}(-\epsilon, t)$, one can see that the distribution function changes significantly from one stationary state, $\mathcal{F}_{\rm neq}(\epsilon)$ [Eq. (44)] on the first half-period, to $1 - \mathcal{F}_{\rm neq}(-\epsilon)$ on the second one (Fig. 8). To produce this change, a large number of electrons, $\sim (A_g - A_g^{\rm ft})/\delta$, should tunnel out from (into) the island during the relaxation stage ($0 < t \lesssim \Gamma_{\mathcal{F}}^{-1}$ and $\mathcal{T}/2 < t \lesssim \mathcal{T}/2 + \Gamma_{\mathcal{F}}^{-1}$ on the two half-periods). This gives a contribution to the leakage current

$$\frac{I_{\rm leak}}{ef} \sim \frac{A_g - A_g^{\rm ft}}{\delta} \gg 1. \tag{46}$$

Moreover, the long interval $\Gamma_{\mathcal{F}}^{-1} \lesssim t < \mathcal{T}/2$, when $\mathcal{F}(\epsilon)$ has already relaxed, contributes even more to the leakage current. Indeed, using the expression (16d) for $I_{\rm leak}$, the estimates $\Gamma_{1-} \sim \Gamma_{2-} \sim \Gamma P_\infty$ from Eq. (16a), and the estimate $\Gamma \sim \Gamma_{1+} \sim \gamma\epsilon_\infty/\delta$, proportional to the number of empty states in the island below the gaps in the electrodes, we estimate the second contribution to the leakage current as

$$I_{\rm leak} \sim e\Gamma_{2-} \sim e\gamma P_\infty \frac{\epsilon_\infty}{\delta} \gg ef. \tag{47}$$

The latter inequality is governed by two large parameters $\epsilon_\infty/\delta \sim (A_g - A_g^{\rm ft})/\delta$ and $\gamma P_\infty/f$.

Among other regions in the (A_g, eV) plane, not corresponding to $\mathcal{F}(A_g - A_g^{\rm ft} < \epsilon < A_g + A_g^{\rm ft}) = 0$, we mention two more, defined by either $\max\{\Delta - eV/2, 3eV/2 - \Delta\} < A_g < \Delta$ with $\epsilon_\infty = A_g - A_g^{\rm ft}$ or $A_g > \Delta + 3eV/2$ with $\epsilon_\infty = A_g - \Delta - eV/2 > eV$. In both these cases the distribution $\mathcal{F}_{\rm neq}(\epsilon)$ coincides on the two half-periods, $\mathcal{F}_{\rm neq}(\epsilon, t < \mathcal{T}/2) = \mathcal{F}_{\rm neq}(\epsilon, t > \mathcal{T}/2)$ being the Fermi-Dirac one in the latter one. Then, the contribution (46) to the leakage, related to the relaxation of $\mathcal{F}(\epsilon)$, vanishes. Still, the stationary leakage current estimated by (47) remains large.

Let us now briefly discuss the quasiequilibrium regime, $\tau_{ee}^{-1} \gg \Gamma_{\mathcal{F}} \gg f, \tau_{eph}^{-1}$, when the distribution function deviates slightly from $\mathcal{F}_{T_e(t)}(\epsilon)$. Generally speaking, one has to take into account the time dependence of the effective electronic temperature $T_e(t)$ governed by (5). However, for the symmetric drive, Eq. (11), and the symmetric device, $C_1 = C_2$, $G_1 = G_2$, $\gamma_1 = \gamma_2 = \gamma$, $-V_1 = V_2 = V/2 > 0$, the steady state values of the electronic temperature in both halves of the period are equal. Variations of $T_e(t)$ in this limit occur only in the short charging/discharging time intervals $\sim 1/\Gamma$ and can be neglected. Then, the treatment of the quasiequilibrium regime is quite analogous to Sec. IV B, with an analogous result (large leakage).

In equilibrium, $\tau_{eph}^{-1} \gg \Gamma_{\mathcal{F}} \gg f$, the electron distribution is Fermi-Dirac. The estimate for the leakage current is then the same as in Eq. (47), with the replacement $\epsilon_\infty \to A_g - A_g^{\rm ft}$, again giving large leakage.

VI. CONCLUSION

We have shown that the accuracy of the pumping current quantization in the turnstile regime of the hybrid SINIS SET is a non-monotonic function of the relaxation rate of the electronic distribution function on the island due to tunneling, $\Gamma_{\mathcal{F}} \sim \gamma\,[P_\infty + f/\Gamma]$. In the equilibrium regime, $\Gamma_{\mathcal{F}} \gg \tau_{eph}^{-1}$, the turnstile current has a plateau $\langle I \rangle \simeq ef$ in the standard interval of driving amplitudes, $A_g^{\rm ft} < A_g < A_g^{\rm bt}$ with the forward and backward tunneling thresholds $A_g^{\rm ft,bt} = \Delta \mp eV/2$. Increase of the tunneling relaxation rate $\Gamma_{\mathcal{F}}$ brings the system into quasiequilibrium at $\tau_{eph}^{-1} \ll \Gamma_{\mathcal{F}} \ll \tau_{ee}^{-1}$, with the effective electronic temperature strongly different from the bath temperature. In this regime, turnstile errors are large except in the small interval near the threshold $A_g/A_g^{\rm ft} - 1 \ll 1$. Surprisingly, at even faster tunneling relaxation rate $\Gamma_{\mathcal{F}} \gg \tau_{ee}^{-1}, \tau_{eph}^{-1}$, when the electronic distribution on the island is essentially non-thermal, the turnstile plateau is recovered, but in a smaller interval of driving amplitudes, $A_g^{\rm ft} < A_g < \Delta$. These considerations hold for sufficiently fast driving frequency, $\Gamma_{\mathcal{F}} \ll f$; in the opposite case, the tunneling processes change the distribution function significantly over the period and lead to a large leakage current.

Such a non-monotonic behavior of the current plateau indicates that the turnstile operation is mostly spoiled by the electron-electron relaxation forming the long-tailed distribution function, but not by the driving itself.

ACKNOWLEDGMENTS

We would like to thank J. P. Pekola for useful discussions. This work has been supported in part by the Nanosciences Foundation under the aegis of the Joseph Fourier University Foundation (Grenoble, France), by the Russian Foundation for Basic Research, and the grant of the Russian Science Foundation (No. 15-12-10020).

[1] F. Giazotto, T. T. Heikkilä, A. Luukanen, A. M. Savin, and J. P. Pekola, Opportunities for mesoscopics in thermometry and refrigeration: Physics and applications. Rev. Mod. Phys. **78**, 217 (2006).

[2] J. P. Pekola, O.-P. Saira, V. F. Maisi, A. Kemppinen, M. Möttönen, Y. A. Pashkin, and D. V. Averin Rev. Mod. Phys. **85**, 1421 (2013).

[3] H. S. Knowles, V. F. Maisi, and J. P. Pekola, Appl. Phys. Lett. **100**, 262601 (2012).

[4] For example, there are such effects as decrease of the quality factors of S resonators[5,6], decoherence in qubit systems[7–9], the excess current in single-electron turnstiles[3], and low efficiency of electronic cooling in normal metal (N) - insulator (I) - superconductor (S) junctions[10,11].

[5] H. Wang, M. Hofheinz, J. Wenner, M. Ansmann, R. C. Bialczak, M. Lenander, E. Lucero, M. Neeley, A. D. OConnell, D. Sank, M. Weides, A. N. Cleland, and J. M. Martinis, Appl. Phys. Lett. **95**, 233508 (2009).

[6] R. Barends, J. Wenner, M. Lenander, Y. Chen, R. C. Bialczak, J. Kelly, E. Lucero, P. OMalley, M. Mariantoni, D. Sank, H. Wang, T. C. White, Y. Yin, J. Zhao, A. N. Cleland, J. M. Martinis, and J. J. A. Baselmans, Appl. Phys. Lett. **99**, 113507 (2011).

[7] J. M. Martinis, M. Ansmann, and J. Aumentado, Phys. Rev. Lett. **103**, 097002 (2009).

[8] H. Paik, D. I. Schuster, L. S. Bishop, G. Kirchmair, G. Catelani, A. P. Sears, B. R. Johnson, M. J. Reagor, L. Frunzio, L. I. Glazman, S. M. Girvin, M. H. Devoret, and R. J. Schoelkopf, Phys. Rev. Lett. **107**, 240501 (2011).

[9] A. D. Còrcoles, J. M. Chow, J. M. Gambetta, C. Rigetti, J. R. Rozen, G. A. Keefe, M. B. Rothwell, M. B. Ketchen, and M. Steffen, Appl. Phys. Lett. **99**, 181906 (2011).

[10] J. P. Pekola, D. V. Anghel, T. I. Suppula, J. K. Suoknuuti, A. J. Manninen, and M. Manninen, Appl. Phys. Lett. **76**, 2782 (2000).

[11] S. Rajauria, H. Courtois, and B. Pannetier, Phys. Rev. B **80**, 214521 (2009).

[12] J. T. Peltonen, J. T. Muhonen, M. Meschke, N. B. Kopnin, and J. P. Pekola, Phys. Rev. B **84**, 220502(R) (2011).

[13] I. Nsanzineza and B. L. T. Plourde, Phys. Rev. Lett. **113**, 117002 (2014).

[14] C. Wang, Y. Y. Gao, I. M. Pop, U. Vool, C. Axline, T. Brecht, R. W. Heeres, L. Frunzio, M. H. Devoret, G. Catelani, L. I. Glazman, and R. J. Schoelkopf, Nature Commun. **5**, 5836 (2014).

[15] U. Vool, I. M. Pop, K. Sliwa, B. Abdo, C. Wang, T. Brecht, Y. Y. Gao, S. Shankar, M. Hatridge, G. Catelani, M. Mirrahimi, L. Frunzio, R. J. Schoelkopf, L. I. Glazman, and M. H. Devoret, Phys. Rev. Lett. **113**, 247001 (2014).

[16] D. J. van Woerkom, A. Geresdi, and L. P. Kouwenhoven, Nature Phys., **11**, 547-550 (2015).

[17] M. Taupin, I. M. Khaymovich, M. Meschke, A. S. Mel'nikov, and J. P. Pekola, Nature Commun. **7**, 10977 (2016).

[18] M. G. Blamire, E. C. G. Kirk, J. E. Evetts, and T. M. Klapwijk, Phys. Rev. Lett. **66**, 220-223 (1991).

[19] D. R. Heslinga and T. M. Klapwijk, Phys. Rev. B **47**, 5157-5164 (1993).

[20] D. J. Goldie, N. E. Booth, C. Patel, and G. L. Salmon, Phys. Rev. Lett. **64**, 954-957 (1990).

[21] H. Q. Nguyen, T. Aref, V. J. Kauppila, M. Meschke, C. B. Winkelmann, H. Courtois, and J. P. Pekola, New J. Phys. **15**, 085013 (2013).

[22] A. Bespalov, M. Houzet, J. S. Meyer, and Y. V. Nazarov, arXiv:1603.04273.

[23] J. P. Pekola, V. F. Maisi, S. Kafanov, N. Chekurov, A. Kemppinen, Yu. A. Pashkin, O.-P. Saira, M. Möttönen, and J. S. Tsai, Phys. Rev. Lett. **105**, 026803 (2010).

[24] O.-P. Saira, A. Kemppinen, V. F. Maisi, and J. P. Pekola, Phys. Rev. B **85**, 012504 (2012).

[25] D. Riste, C. C. Bultink, M. J. Tiggelman, R. N. Schouten, K. W. Lehnert, and L. DiCarlo, Nature Comm. **4**: 1913 (2013).

[26] H. Pothier, S. Gueron, N. O. Birge, D. Esteve, and M. H. Devoret, Phys. Rev. Lett. **79**, 3490 (1997); *ibid* Z. Phys. B **104**, 178 (1997).

[27] M. A. Laakso, T. T. Heikkilä and Y. V. Nazarov, Phys. Rev. Lett. 104, 196805 (2010)

[28] J. P. Pekola, T. T. Heikkilä, A. M. Savin, J. T. Flyktman, F. Giazotto, F. W. J. Hekking, Phys. Rev. Lett. **92**, 056804 (2004).

[29] F. Giazotto, T. T. Heikkilä, F. Taddei, Rosario Fazio, J. P. Pekola, F. Beltram, Phys. Rev. Lett. **92**, 137001 (2004).

[30] J. P. Pekola, J. J. Vartiainen, M. Möttönen, O.-P. Saira, M. Meschke, and D. V. Averin, Nature Physics **4**, 120 (2008).

[31] B. Kaestner and V. Kashcheyevs, Rep. Prog. Phys. 78, 103901 (2015)

[32] D. M. T. van Zanten, D. M. Basko, I. M. Khaymovich, J. P. Pekola, H. Courtois, C. B. Winkelmann, Phys. Rev. Lett. **116**, 166801 (2016).

[33] I. L. Aleiner, P. W. Brouwer, and L. I. Glazman, Phys. Rep., **358**, 309 (2002).

[34] D. V. Averin, A. N. Korotkov, JETP **70**, 937 (1990) [Zh. Eksp. Teor. Fiz. **97**, 1661 (1990)].

[35] D. V. Averin, A. N. Korotkov, J. Low. Temp. Phys. **80**, 173 (1990).

[36] Strictly speaking, since both electron-electron and electron-phonon collisions conserve the total number of electrons on the island, both limiting equilibrium distributions should be taken with some chemical potential, chosen to give the same total number of electrons as the distribution $\mathcal{F}(\epsilon)$. However, in this work we consider only two values of this total number, so the chemical potential may vary only by a small amount $\sim \delta$, which we neglect.

[37] U. Sivan, Y. Imry, and A. G. Aronov, Europhys. Lett. **28**, 115 (1994).

[38] Ya. M. Blanter, Phys. Rev. B **54**, 12807 (1996).

[39] F. C. Wellstood, C. Urbina, and J. Clarke, Phys. Rev. B **49**, 5942 (1994).
[40] A. Sergeev and V. Mitin, Phys. Rev. B **61**, 6041 (2000).
[41] V. I. Yudson and V. E Kravtsov, Phys. Rev. B **67**, 155310 (2003).
[42] D. M. Basko and V. E. Kravtsov, Phys. Rev. B **71**, 085311 (2005).
[43] A. Sergeev, M. Yu. Reizer, and V. Mitin, Phys. Rev. Lett. **94**, 136602 (2005).
[44] M. Prunnila, P. Kivinen, A. Savin, P. Törmä, and J. Ahopelto, Phys. Rev. Lett. **95**, 206602 (2005).
[45] D. V. Averin and J. P. Pekola, Phys. Rev. Lett. **101**, 066801 (2008).
[46] Here we neglect the exponentials $e^{-\Delta/T-c_0(A_g-\Delta\pm eV/2)/(A_g-A_g^{\rm ft})}$ due to the smallness of the bath temperature $T<T_e/2$.
[47] M. A. Laakso, P. Virtanen, F. Giazotto, and T. T. Heikkilä, Phys. Rev. B **75**, 094507 (2007).
[48] Although aluminum itself is superconducting at low temperatures and cannot be used as a material for a normal island, a small admixture of Mn around $0.1-0.3$ % suppresses the critical temperature of the AlMn alloy down to 50 mK (Refs. 49 and 50). Such a small amount of Mn impurities does not significantly change the thermal properties of the material such as heat capacity.[49] We also use the unchanged value of $\Sigma=0.2\cdot10^9$ J K^{-5} m^{-3} taken for Al, although there are some indirect indications of larger Σ values in this material (see, e.g., Ref. 51), but we are not aware of any direct measurements of the electron-phonon coupling constant in AlMn.
[49] S. T. Ruggiero, A. Williams, W. H. Rippard, A. Clark, S. W. Deiker, L. R. Vale, and J. N. Ullom, J. Low Temp. Phys., **134**, 973 (2004).
[50] G. ONeil, D. Schmidt, N. A. Miller, J. N. Ullom, A. Williams, G. B. Arnold, and S. T. Ruggiero, Phys. Rev. Lett., **100**, 056804 (2004).
[51] A. M. Clark, A. Williams, S. T. Ruggiero, M. L. van den Berg, and J. N. Ullom, Appl. Phys. Lett., **84**, 625 (2004).
[52] A. Kemppinen, S. Kafanov, Yu. A. Pashkin, J. S. Tsai, D. V. Averin, and J. P. Pekola, Appl. Phys. Lett. **94**, 172108 (2009).

Appendix A: Verification of the assumption $\mathcal{F}_0(\epsilon,t)=\mathcal{F}_1(\epsilon,t)$

To verify the validity of the assumption that the n-dependence of the distribution functions $\mathcal{F}_n(\epsilon)$ is negligible, one has to start with the rate equations for the full density matrix, see Eqs. (3) in Ref. 34. For $n=0,1$ within the assumption of the energy scale separation $E_C\gg\delta$, one can rewrite these equations in the form of Eq. (2a) and the kinetic equations for the distribution functions $\mathcal{F}_0(\epsilon)$ and $\mathcal{F}_1(\epsilon)$:

$$\begin{aligned}p_0\dot{\mathcal{F}}_0&=\Gamma_-p_1(\mathcal{F}_1-\mathcal{F}_0)\\&+\gamma p_0(t)\sum_{\eta=\pm}n_S^+\left(-\mu(t)+\eta\tfrac{eV}{2}-\epsilon\right)\mathcal{F}_0(1-\mathcal{F}_0)\\&+\gamma p_1(t)\sum_{\eta=\pm}n_S^+\left(\mu(t)-\eta\tfrac{eV}{2}+\epsilon\right)\mathcal{F}_1^2,\end{aligned}\tag{A1}$$

$$\begin{aligned}p_1\dot{\mathcal{F}}_1&=\Gamma_+p_0(\mathcal{F}_0-\mathcal{F}_1)\\&+\gamma p_0(t)\sum_{\eta=\pm}n_S^+\left(-\mu(t)+\eta\tfrac{eV}{2}-\epsilon\right)(1-\mathcal{F}_0)^2\\&+\gamma p_1(t)\sum_{\eta=\pm}n_S^+\left(\mu(t)-\eta\tfrac{eV}{2}+\epsilon\right)\mathcal{F}_1(1-\mathcal{F}_1),\end{aligned}\tag{A2}$$

where $\Gamma_\pm=\sum_j\Gamma_{j\pm}$. As we will show below, the relaxation time to the state $\mathcal{F}_0(\epsilon,t)=\mathcal{F}_1(\epsilon,t)\equiv\mathcal{F}(\epsilon,t)$ is of the same order as the charge relaxation time Γ^{-1} which is much shorter than all other characteristic times.

For this purpose let us consider the beginning of the injection stage. Just before this stage, the island has been discharged, therefore $p_1(0)\simeq P_\infty\ll1$, while $p_0(0)\simeq1$. As we suddenly changed $\mu(t)$ from $-A_g$ to A_g we made $\Gamma_+\simeq\Gamma\gg\Gamma_-,\gamma$. As a result, all the rates in (A1) are much smaller than Γ, so we can consider $\mathcal{F}_0(\epsilon,t)=\bar{\mathcal{F}}_0(\epsilon)$ to be constant at this time scale. On the other hand, the first term on the right-hand side of Eq. (A2) is dominant at such short times, and one can rewrite this equation as follows:

$$\frac{d(p_1\mathcal{F}_1)}{dt}=\Gamma_+p_0\bar{\mathcal{F}}_0-\Gamma_-\cdot(p_1\mathcal{F}_1)\ ,\tag{A3}$$

where we used the equation

$$\frac{dp_0}{dt}=-\Gamma_+p_0+\Gamma_-p_1\tag{A4}$$

with the solution (14a) $p_0(t)\simeq P_\infty+(1-2P_\infty)e^{-\Gamma t}$, and neglected an exponentially small correction $e^{-\Gamma\mathcal{T}/2}$.

Finally, integrating (A3) at $t\lesssim\Gamma^{-1}$, one can find

$$\mathcal{F}_1(\epsilon,t)=\bar{\mathcal{F}}_0+\frac{P_\infty(\mathcal{F}_1(0)-\bar{\mathcal{F}}_0)e^{-\Gamma_-t}}{P_\infty+(1-2P_\infty)(1-e^{-\Gamma t})}\ .\tag{A5}$$

One can see that the function $\mathcal{F}_1(\epsilon,t)$ relaxes from any initial value $\mathcal{F}_1(0)$ to the final one $\simeq\bar{\mathcal{F}}_0+P_\infty[\mathcal{F}_1(0)-\bar{\mathcal{F}}_0]$, which is close to $\bar{\mathcal{F}}_0$, on the time scale Γ^{-1} with a subsequent relaxation at larger time scales.

Eventually neglecting such small difference $P_\infty=\Gamma_-/\Gamma\ll1$ and working at larger time scales $\Gamma t\gtrsim1$ one can put $\mathcal{F}_0(\epsilon,t)=\mathcal{F}_1(\epsilon,t)\equiv\mathcal{F}(\epsilon,t)$.